Bull. Chem. Soc. Ethiop. **2025**, 39(3), 585-600.
DOI: https://dx.doi.org/10.4314/bcse.v39i3.15

ISSN 1011-3924
Printed in Ethiopia
Online ISSN 1726-801X

COMPUTATIONAL DETAILS OF MOLECULAR STRUCTURE, SPECTROSCOPIC PROPERTIES, DFT CALCULATIONS AND MOLECULAR DOCKING STUDY OF SOME 1,4-DISUBSTITUTED-1,2,3-TRIAZOLE DERIVATIVES DERIVED FROM 4-AMINOBENZEN SULFONIC ACID

Hawraa Abdul Kadhim Mazyed[1], Noor Hameed Imran[1], Shaymaa Adil Mohammed[1], Murad G. Munahi[2*] and Riyadh J. Nahi[1,3]

[1]Department of Chemistry, College of Science, Al-Muthanna University, Iraq
[2]Department of Biology, College of Science, Al-Muthanna University, Iraq
[3]College of Pharmacy, Al-Muthanna University, Iraq

(Received July 16, 2024; Revised November 20, 2024; Accepted November 22, 2024)

ABSTRACT. In the current study, structural optimization, electronic, vibrational properties and molecular docking simulation were investigated for two 1,4-disubstituted-1,2,3-triaozle derivatives (A and B). The theoretical spectroscopic analytical results of IR, NMR and UV–Vis were obtained using DFT methods, and the predicted results were compared to the experimental results reported in the literature. To forecast the highly electron-dense locations of the compounds, the molecular electrostatic surface potential, (MEP) was analyzed; and the quantum and chemical characteristics were computed. A thorough discussion of topological analysis using the reduced density gradient (RDG) was conducted. Moreover, to predict (*in silico*) the antiviral behavior of the reported heterocyclic compounds A and B, the crystal structures of the viral hepatitis C (6UE3 and 8DK6) were subjected to molecular docking simulation. The binding affinity between the heterocyclic ligands and the target proteins was investigated using molecular docking. The results showed that the triaozle derivatives have a good binding energy toward the virus target 8DK6 (-7.16 and -7.03 kcal/mol) for compound A and B, respectively. Herein, we introduce two triazole derivatives as potential anti-HCV.

KEYWORDS: 1,2,3-Triazole, Computational study, DFT, In silico, Molecular docking, HCV

INTRODUCTION

The 1,2,3-triazole ring belongs to a family of organic heterocyclic molecules that have received a special attention due to their applications in different pharmaceutical fields, such as anti-microbial [1], antiviral [2], analgesic [3], antidiabetic [4], antimalarial [5], anti-oxidants [6], antibacterial [7], anticancer [8], and anti-neoplastic [9]. Structurally, 1,2,3-triazole is an aromatic five-membered and π-excessive nitrogen containing heterocycle with 6π electrons ring system comprised of three regular nitrogen and two carbon atoms with two double bonds [10, 11]. Thus, all the atoms in 1,2,3-triazole ring are sp^2 hybridized where the available 6π electrons are delocalized around the ring and one of the nitrogen atoms is a pyrrole type while the other two are pyridine types [12]. In addition, the ionization energy of 1,2,3-triazole is 10.06 eV [13]. Functionally, heterocycles can bind to the target proteins by forming a variety of non-covalent interactions with different amino acid residues such as hydrogen bonds [14], π–π aromatic stacking [15], hydrophobic effects [16], salt bridges [17], and cation–π interactions [18]. Therefore, studying the geometrical and energetic characteristics of these non-covalent interactions is particularly important for various applications of drug discovery. On the other hand, computational studies are essential for examining the molecular structure and electronic properties of a diverse array of highly functionalized molecules such medicines [19]. The in-depth computational experience was derived from utilizing advanced wave function methods, such as

*Corresponding authors. E-mail: muradmunahi@mu.edu.iq

density functional theory (DFT) which is the most popular assay to understand the relations between the structural and biological, electronic, topological, spectroscopic properties of the ligands [20]. In addition, molecular docking is a computational technique predicts the binding affinity of small molecules (ligands) toward target proteins [21]. The docking score function of ligand-protein interaction estimates several non-covalent interactions, which allows to describe the behavior of ligands in the binding site of target proteins in addition to explain fundamental biochemical processes [22]. Therefore, in bioinformatics and drug design, the former type of interactions between protein and ligands provides some intriguing insights into regulation and inhibition of enzymes [23]. Considering previous efforts in prospective categories of heterocyclic compounds such as triazoles, recent advances in treating various types of cancer diseases including pancreatic, colon, cervical, and breast cancers have been documented through several literatures [24-26]. Also, it was discovered that some heterocyclic compounds derived from triazoles demonstrated particular efficacy in DNA cleavage suppression and reducing angiogenesis [27].

The current study aimed to investigate the geometrical, electronic molecular properties and enzyme inhibition activity of two previously synthesized and characterized heterocyclic compounds A and B (Figure 1) as described in the literature [28].

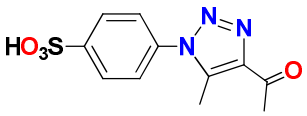

4-(4-Acetyl-5-methyl-1H-1,2,3-triazol-1-yl) benzenesulfonic acid.

A

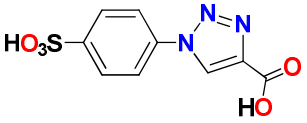

1-(4-Sulfophenyl)-1H-1,2,3-trizole-4-carboxylic acid

B

Figure 1. The chemical structure of recently synthesized heterocyclic compounds [24].

EXPERIMENTAL

Computational details

Computational studies using DFT were achieved for the synthesized 1,2,3-triazole compounds A and B. Optimized geometrical and electronic calculations based on DFT were conducted using the Lee Yang Parr (B3LYP) method [29, 30], with the basis set 6-311G++ (d,p), using Gaussian 09 software [31]. The Gaussian input file generation and visualization of the optimized structure were achieved using GaussView software v6.0 [32] and Avogadro program [33]. The studied compounds were characterized computationally using time-dependent density functional theory (TD-DFT) with CPCM solvation model calculations. ^{1}H-NMR and ^{13}C-NMR spectral data were computationally predicted using DFT/B3LYP/6-311G(d,p), and following GIAO method. The chemical shift was referenced to TMS as a standard. Topological analysis was considered because it aids in discovering atom-atom interactions at the structure's surface. To identify the electrophilic and nucleophilic binding sites, molecular electrostatic potential (MEP) was used. The analysis of non-covalent interactions was conducted using the reduced density gradient (NCI-RDG) method, which aids in illustrating the type of intramolecular interactions. All softwares were used with default parameters. The calculated parameters are described by the ensuing equations [34].

Ionization potential (I) = −EHOMO (1)

Electron affinity (A) = −ELUMO (2)

Chemical hardness (η) = (I − A)/2 (3)

Chemical potential (μ) = −(I + A)/2 (4)

Electronegativity (χ) = −(EHOMO + ELUMO)/2 (5)

Electrophilicity index (ω) = μ2/2η (6)

Global softness (S) = 1/2η (7)

Docking studies

Based on the ligands' likelihood, two target proteins were selected. The two targets are hepatitis C virus's (PDB id: 6ue3; resolution 1.56 Å) and (PDB id: 8dk6 and; resolution 2.45 Å), were retrieved in (pdb) format from protein data bank (RCSB PDB: Homepage) [35, 36]. The hepatitis C virus's proteins (6ue3 and 8dk6, chain A) were docked with the optimized compounds (A and B) as well as Ribavirin which used as a reference ligand, in order to evaluate the strength of the resulting contact. The three-dimensional structures of compounds were built using the Avogadro software. A molecular docking simulation was conducted using AutoDock tools = 1.5.6 software [37]. First, the selected target protein was prepared by removing any water molecules, extra ions, or ligands not specified in the study protocol. Polar hydrogens and Gasteiger charges were added to the protein. BIOVIA Discovery Studio Visualizer (v.4.5) (http://www.accelrys.com) was used to visualize the intermolecular interactions between the proteins and ligands, with the grid center set at (X = -12.78, Y = -17.93, Z = 12.80) and (X = 43.997, Y = -1.104, Z = 37.578) for 6UE3 and 8DK6, respectively.

RESULTS AND DISCUSSION

DFT calculations

Optimization and geometrical structure

The calculated geometrical parameters (bond lengths and bond angles) for both 1,2,3-triazole structure are illustrated in Table S1 (Supplementary file), these parameters can assist in describing the structural substituents on the parent system. In the structure of ligand, A, 1,2,3-triazole is bearing acetyl and methyl groups attached at 4- and 5-positions, respectively. While in ligand B, 1,2,3-triazole ring system containing only carboxyl group attached at 4-position. This difference may exert some structural changes in the system. Additionally, these later groups are electron donating entities can motivate some intramolecular interactions. Also, another structural effect, the presence of two methyl groups seems to be in the same plane, this makes some steric effect leading to optimum location for one group in front and closed to phenyl remaining part. The bond length values of some focused substituents vary from 1.089 Å (C16-H27) to 1.494 Å (C15-C16). Furthermore, bond angle values ranged from 103.602o (N11-C15-C14) to 133.029o (C14-C15-C16). Considering the system B, triazole-bearing carboxylic group was associated with some geometric variation. Besides, the electron-attracting COOH group caused the more positively charged hydrogen atom to be positioned closer to the nitrogen atoms of the triazole ring, suggesting the formation of a hydrogen bond. This observation can give some stability of the system. Bond length values can be ranged from 1.075 Å (C11-H23) to 1.482 Å (C10-C12), and the bond angle values were ranged from 104.21o (N7-C11-C10) to 131.56o (C10-C11-C23).

Computational comparison for spectroscopic properties

IR spectral analysis

In this investigation, the molecular structure of the studied ligands was verified by analyzing vibrational IR spectra via computational calculations. Quantum mechanics methods heavily rely on harmonic potentials. However, to ensure accurate comparison with experimental data, a correction step is necessary. The investigated data needs to be multiplied by a scale factor of 0.967 for calibration purposes. This will ensure that the computational results match the experimental data, allowing for more precise analysis (https://cccbdb.nist.gov/vibscalejust.asp). In case of ligand A, the sulfonyl hydroxide group exhibits a distinct band peak at 3647 cm^{-1}, while experimentally [28], a broader peak with less intensity is observed within the range of (3506-2900) cm^{-1}, compared to its theoretical data, IR spectra of hydroxyl-containing compounds can be obtained without observing this broad signal. Small bands appear at (3097 and 3038) cm^{-1} corresponding to Ar-C-H and aliphatic C-H, respectively. In contrast, the experimental data indicate the appearance of an absorption band at (3068 and 2920) cm^{-1}. In addition, the theoretical results exhibit a distinct absorption band at 1701 cm^{-1}, which is attributed to the carbonyl group. This result is in close agreement with the experimental data. Additionally, the absorption band at 1371 cm^{-1} indicates the presence of an (N=N) triazolyl ring, which matches the experimental finding. Regarding ligand B, the absorption band at (3646 and 3577) cm^{-1} is attributed to the hydroxyl group of sulphonic acid and carboxylic acid groups respectively; but, in the experimental data, the hydroxyl peak of the sulphonic acid and carboxylic acid overlap, causing the IR peak to appear broadened. The absorption band at 1767 cm^{-1} is attributed to the carbonyl group, this result closely aligns with the experimental data at the absorption band of 1722 cm^{-1}. Most of computational data evaluated aligned with the experimental results.

UV–Vis electronic spectra using TD DFT method

The electronic behavior of 1,2,3-triazole compounds A and B were showed UV-Visible peaks at wavelengths between 200 and 400 nm, as illustrated in Figure 2. Band attribution is based on the transition energy scale involved between several molecular orbitals (MOs). Furthermore, oscillator strengths (F) can measure the power of electronic transition between each two MOs. The default settings in Gaussian 09 were modified to N state = 6 to analyze six states. The type of transition mainly controlled with an energetic gap quantity, consequently, the current ligands exhibit six excitation energies. The absorption band is observed to vary between strong, medium, and weak. The detailed LOG Gaussian file provides an image of the first and second transition, which corresponds to a singlet strong absorption band. For ligand A, TD-DFT protocol detected the most suitable electronic transitions up to 6 transitions. A significant orbital contribution was obvious with HOMO → LUMO for third line transition (λ_{max} = 257.72 nm) corresponding to transition energy of 4.8108 eV and F value of 0.3153. While ligand B showed a significant contribution for first line HOMO → LUMO electronic transition (λ_{max} = 258.39 nm) corresponding to transition energy of 4.7983 eV and F value of 0.6584. Mostly, the electrons involved in this excitation related to n- π* and π- π* transition types and that achieve the stability of the studied compounds. Electronic circular dichroism (ECD) is a spectroscopic technique can reveal details on the chiral and electronic transitions of molecules. It is particularly helpful for exploring the characteristics and structure of chiral compounds. By plotting ellipticity versus wavelength, an ECD spectrum is obtained, which is more sensitive to electrode potential than a UV–vis spectrum [38]. In the case of ligand A, the theoretical results record various ECD bands and R_{vel} (rotatory strengths velocity), appearing as a positive ECD band at 257.72 nm and R_{vel} 15.84, due to the peak being at a higher wavelength λ_{max} 302.44 nm. There are two very intense negative bands at ca. 259.39 and 242.68 nm and R_{vel} at -40.46 and -59.46, respectively. The bands

in the 236.66, 249.09, and 302.44 nm range manifest themselves as a negative band pattern. As for ligand B, there are two positive ECD bands at 258.39 nm, R_{vel} 45.29 and 254.44 nm, R_{vel} 17.39, respectively. Additionally, it showed four negative ECD bands at 223.58, 229.37, 233.28, and 241.53 nm and R_{vel} -57.14, -7.19, -7.29, and -2.61, respectively (Figure 3). The variation in peak position and intensity signifies distinct molecular configurations [39].

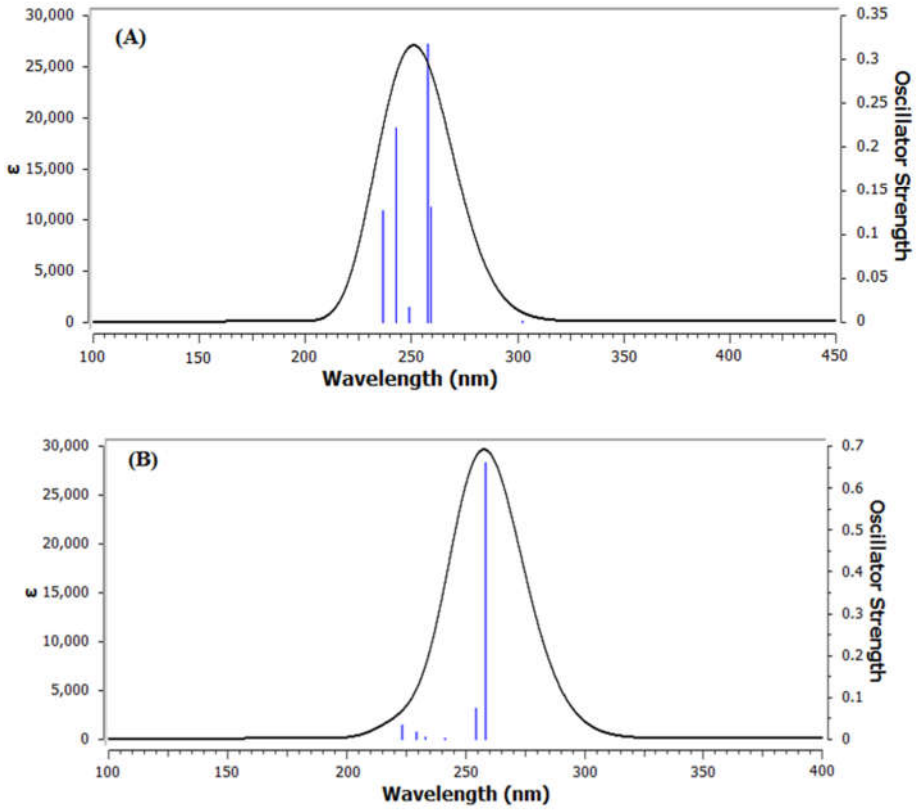

Figure 2. The predicted absorption spectra (UV–Vis) of the heterocyclic compounds: (A) ligand A and (B) ligand B.

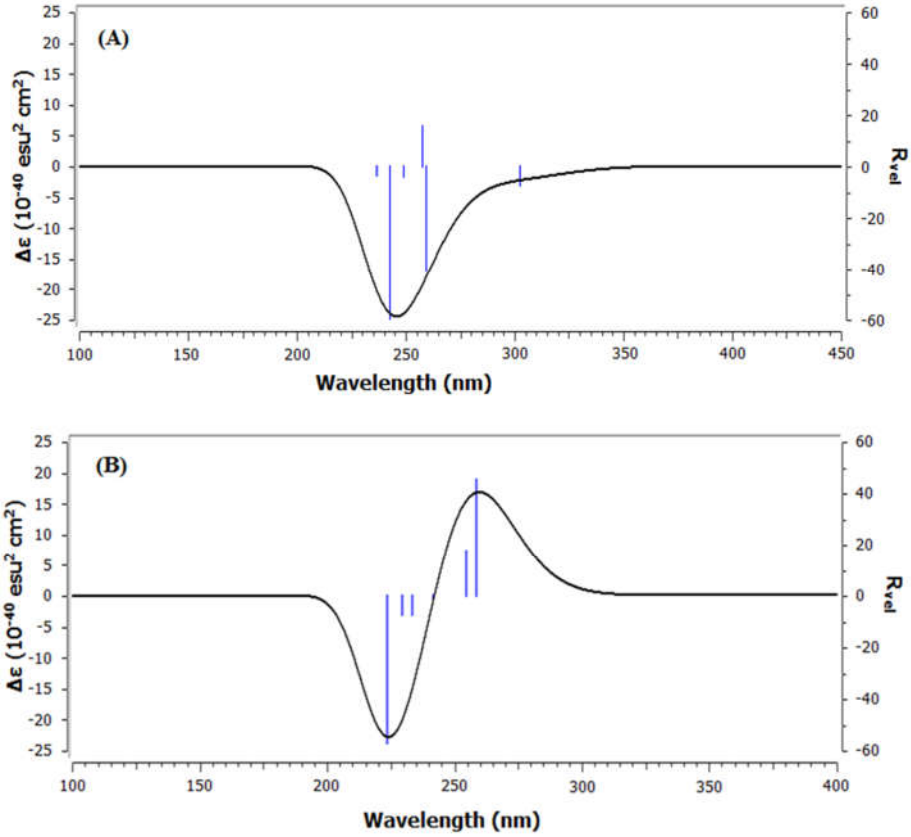

Figure 3. The predicted absorption spectra (ECD) of the heterocyclic compounds: (A) ligand A and (B) ligand B.

^{1}H and ^{13}C NMR spectral investigation

NMR studies offer detailed insights into the structures and conformations of small molecules, proteins, and ligand-protein complexes, including their dynamic behavior. This information is crucial for the discovery and development of new pharmaceutical compounds. The ^{1}H and ^{13}C NMR in DMSO as a solvent were predicted for the compounds 1,2,3-triazole (A and B) after optimization using B3LYP/ 6-311G ++(d,p). In the case of ligand, A, the chemical shifts ^{1}H NMR for H20, H21, H22 and H23 belonging to the aromatic protons were calculated to be 7.9-8.4 ppm while the corresponding experimental signals were observed at 7.5-7.8 ppm [28]. Also, for (H25-H30) its position appears at 2.1-2.9 ppm matching the reported experimental data 2.5-2.6 ppm. The theoretical ^{13}C NMR spectrum was close to the reported experimental data. As for ligand B, the calculated result of the chemical shift of H24 for the carboxylic group was present at 9.08 ppm and the chemical shift for H25 of the sulphonic acid group was calculated at 5.5 ppm, while experimentally it was absent, the reason could be attributed to several factors, one possible reason could be establishing of hydrogen bonds between the OH group and other molecules, leading to changes in the chemical environment and resulting in a shift or broadening of the OH peak in the

spectrum [40]. The H23 shows the same value as the triazole ring proton theoretically and experimentally. Aromatic protons H19, H20, H21 and H22 appeared at 8.6-8.1 ppm and were less different from reported experimental data at 7.9-7.8 ppm, which is attributed to the medium conditions in which the calculations or experiments were conducted (solvent effect). ^{13}C NMR spectral data, the carbon of COOH was predicted to be 163.7 ppm while the corresponding experimental signal was observed at 161.5 ppm, according to the predicted spectrum analysis, the signals position of other carbon atoms varied based on their surrounding environment, and most of the data closely matched the reported experimental results [28].

Quantum and reactivity parameters

To investigate the electronic behavior of compounds A and B, the chemical reactivity parameters, including Frontier molecular orbital (FMO) energies, electronegativity (χ), ionization potential (I), electron affinity (A), dipole moment (D), chemical potential (μ), chemical hardness (η) and global softness (S), were calculated. FMOs generally consist of two types of orbitals, the highest occupied molecular orbital (HOMO) and the lowest unoccupied molecular orbital (LUMO) that reflect the reactivity and stability of compounds. The low E_{LUMO} value explains the molecule's low resistance to accepting electrons, while the high E_{HOMO} value illustrates how easily the compound donates an electron to the molecule's unoccupied orbital that serves as a receptor. The differences between FMO (HOMO-LUMO) energies are known as the energy gap (E). The E_{HOMO} and E_{LUMO} parameters, which are useful in predicting a molecule's capacity to give or accept electrons, are related to both I and A values. Structure A had a greater E (4.762 eV), indicating higher stability and forming a compound with less reactivity. The structure of compound B, in contrast, has a smaller energy gap (2.123 eV), indicating greater reactivity and less stability. I and A parameters act as the foundation for the global reactivity descriptors (chemical hardness and global softness). The electrophilicity index (ω), which is determined by the formula = $\mu 2/2\eta$, estimates the energy change that occurs when the system becomes electron-saturated. $S = 1/2\eta$ is used to calculate the overall softness. Figure 4 demonstrates that the electronic orbital densities dispersed on the HOMO and LUMO of the examined compounds involve the triazole ring system and carbonyl group, the possibility of an electron transition from the HOMO to LUMO levels is ensured by this dispersion.

Natural bond orbital (NBO) analysis

The electrophilic and nucleophilic centers of the molecule can be identified by using charge calculations to predict the electron-dens and electron-poor sites in the molecule. According to the analysis of the NBO calculation, Figure 5 depicts the 2D-schema of the investigated ligands carrying charges on each heteroatom. Oxygen atoms of sulfonic acid group in both ligands A and B are higher negative charge than nitrogen atom, therefore sew most interactions between ligand and protein in molecular docking occurred at this part. In ligand (A), the greater negative charge on the O19, N11, and N13 atoms causes them to act as nucleophilic centers compared to N12. Also, in ligand (B) the electron-rich center present on O13, O14 of carboxylic group and N7 and N9 of 5-memebered ring, rather than S atom which has less electronegativity than nitrogen atom. The electrophilic centers mainly caused by oxygen and nitrogen atoms in both ligands.

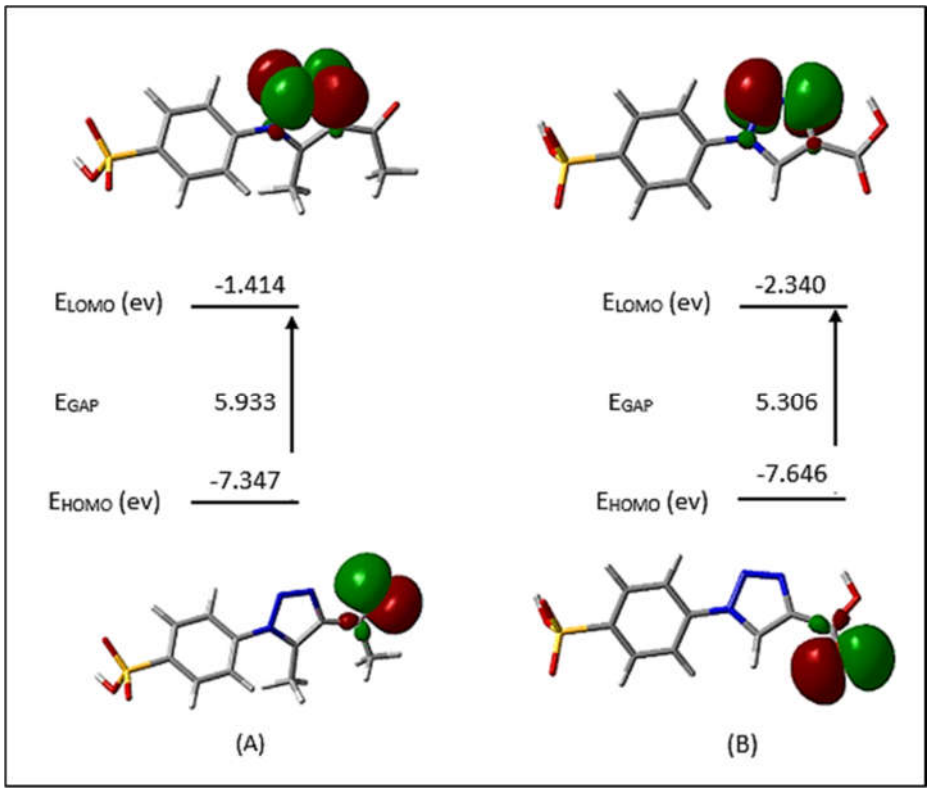

Figure 4. Electronic distribution of FMOs for the optimized compounds of A and B structures.

Molecular electrostatic potential (MEP)

Figure 6 shows the colored map of MEP for the examined compounds A and B, where the electron density varies from red to blue, indicating the highest to lowest electron density on the surface. The negative potential was assigned to the O19 atom in A structure, which represents the active sites, making it possible to synthesize heterocyclic compounds [41, 38]. Additionally, the triazole ring system's N11, N12, and N13 atoms have high negative potential in contract, while the triazole ring in the B structure has medium negative potential. The MEP of the B structure revealed that the density of charge delocalized on the two oxygen atoms of the carboxyl group and the oxygen atoms of the A compound of the ketone group a, due to this electron-rich coordination the electronic system stabilized.

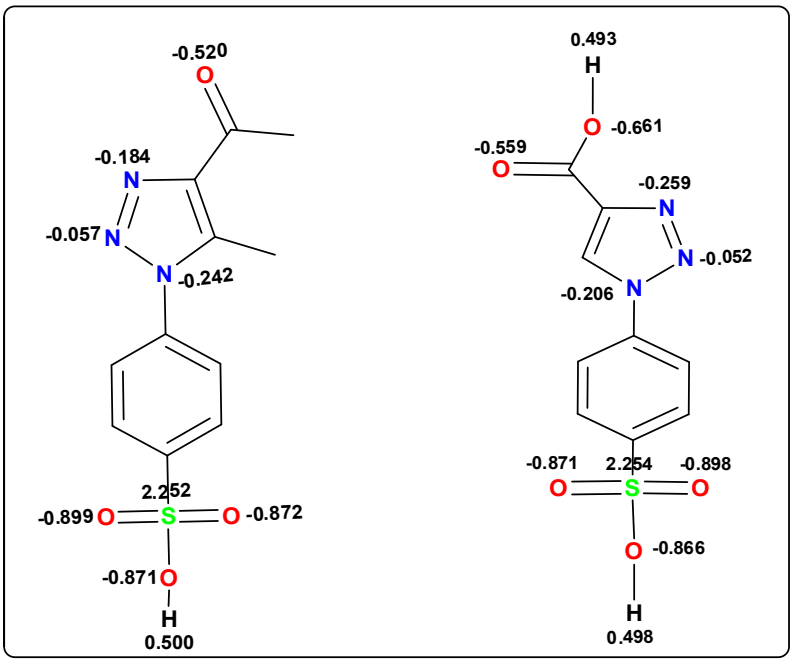

Figure 5. 2D-structure of studied compounds (A and B) with charge of each heteroatoms using DFT/B3LYP method.

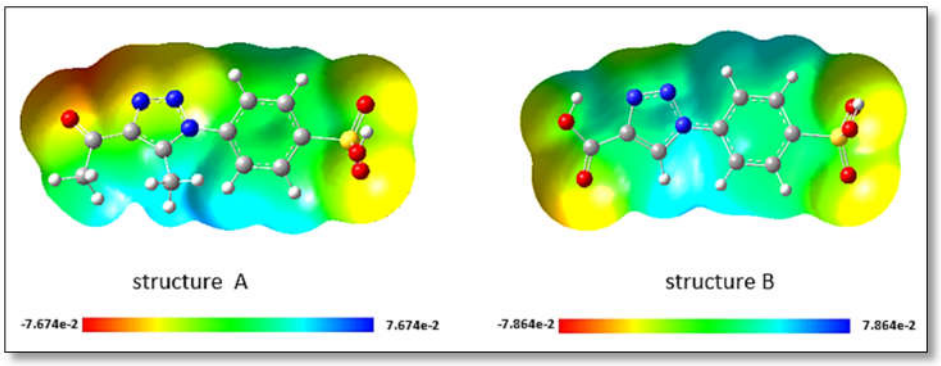

Figure 6. MEP surface of the optimized structures of the heterocyclic A and B structures.

The average local ionization energy (ALIE)

A key element in characterizing the electronic surface of molecules is the average local ionization energy (ALIE). ALIE is the amount of power required to zap an electron from a system's point r. The color code calculated from the ALIE map can be used to demonstrate electrophilic behavior. For the systems under study, the electron-rich sites with low ALIE values are represented by a

blue color with cyan points depicting the ease electronic removal. Mainly, the most important entities in both systems are the sulphonic groups which initiate the electron removing capability. Particularly, structure A obviously draws a dramatic map involving some more electronic density distributed along the system. This observation can estimate for structure A as an electronic rich reactive system compared with structure B.

RDG scatter plots and non-covalent interaction (NCI) analysis

Non-covalent interaction analysis (NCI) predicts non-covalent bonds between molecular atoms and examines the interaction behavior of atomic sites with other molecular atoms. Reduced density gradient analysis is evaluated using the (sign λ2)ρ parameter, which represents the product of the electron density and the sign of the second Hessian eigenvalue [33]. To demonstrate the types of interactions, the colors code was reported as follows: Blue indicates hydrogen bond formation, green signifies Van der Waals attraction, and red denotes steric repulsion interactions. As elaborated from Figure 7, the attractive mapped areas focussed in the cage of triazole ring with either OH of compound A or CH_3 of compound B. However, the most electrostatic interaction occurs with the two methyl groups in compound B reaching to some structure stability. H-bonds were predicted to be absent in both compounds due to the specific geometrical locations.

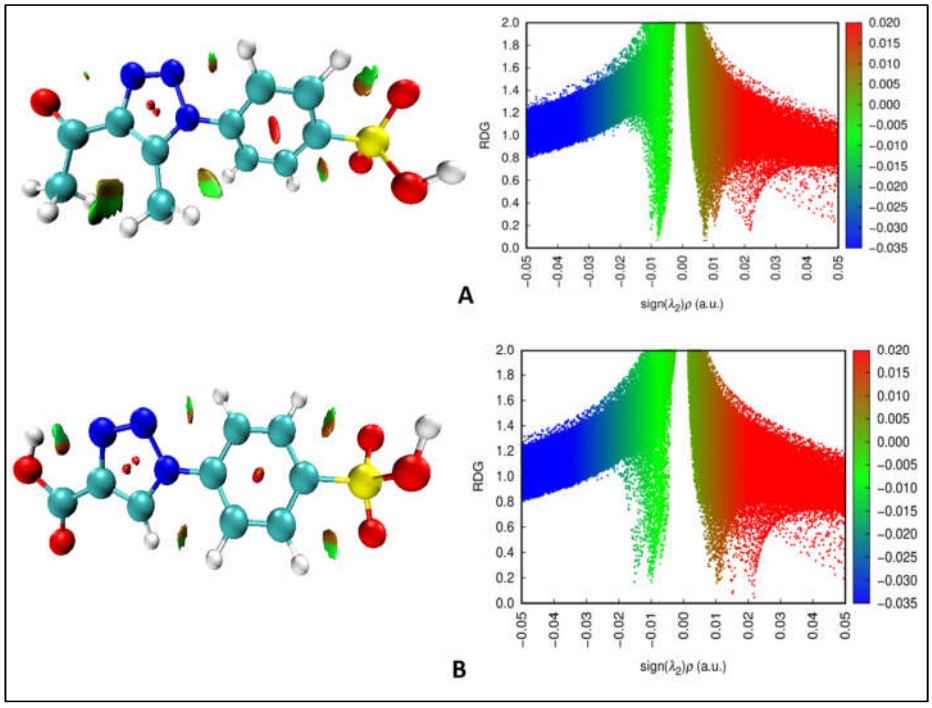

Figure 7. NCI isosurfaces and RDG scatter plot diagram of the optimized structures (A and B).

Molecular docking studies

Molecular docking aims to simulate the potential of a small molecule to block or inhibit a biomolecule such as enzymes, thereby predicting the small molecule's bioactivity. The binding affinity refers to the binding energy between a small molecule and macromolecule. The number of H-bonds, hydrophobic forces, polar and non-polar contacts, and van der Waals interactions were used to assess the binding energy of the ligand towards target proteins. For the molecular docking investigation, 6UE3 and 8DK6 were employed as target proteins in the simulation. NS3/4A protease (6UE3), which is an essential viral enzyme required for HCV replication and maturation was selected as a target, this enzyme considered as an excellent target for discovering anti-HCV. It was found from the docking analysis that there was noticeable differences between the commercial drug ribavirin (C) and the selected compounds (A) and (B) since the observed binding affinities of compounds (A and B) were higher than those of the control drug (C) and for both targets (6UE3 and 8DK6) as shown in Table 1. The docking conformations with the lower binding energy, corresponding to higher affinity, were subjected for additional visualization in order to obtain the best conformation. Table 1 displays the docking score and key interacting amino acid residues along with their binding distances. According to the results, Ligand A and B formed three hydrogen bonds with the target 6UE3 via Gln1041, Gly1137, and Ser1139, this residue is involved in the active site of 6UE3 which is composed of several key residues including: Gln1041, Thr1042, Phe1043, Val1055, Tyr1056, His1057, Gly1058, Val1078, Asp1081, Arg1123, Ile1132, Leu1135, Lys1136, Gly1137, Ser1138, Ser1139, Phe1154, Arg1155, Ala1156, Ala1157, Val1158, Ser1159, Ala1168. In addition to hydrogen bonding, ligand A formed other multiple interactions such as van der Waals and Pi-Cat ion with an appropriate positioning inside the active site. The docking scores were -6.51, -6.64, and -6.32 kcal/mol for compounds A, B, and standard drug respectively. On the other hand, compound A positioned inside the active site of 8DK6, the hydrogen bond was formed through Ser113, while for compound B no hydrogen bonding was observed, however weak bonding, such as van der Waals, result in a highly cooperative behavior, where a variety of bonds work together to create robust molecular clusters. This leads to the formation of stable interactions between the ligand and protein [44, 45]. The docking scores in this case were -7.16, -7.03 and -6.03 kcal/mol, for ligand A, B, and standard drug respectively. Based on the obtained results compared with the standard drug ribavirin, both ligands could be considered as a potent anti-HCV agent, where the studied compounds and control drug were positioned at the active sites of both selected macromolecular targets, as shown in Figures 8 and 9.

Table 1. Binding energy of the optimized 1,2,3-triazole ligands complexed with 6UE3 and 8DK6.

Protein-ligand complex	Binding energy (kcal/mol)	Protein residues involved in intermolecular interactions
A +6UE3	-6.51	Gln1041, Thr1042, Phe1043, Val1055, His1057, Gly1058, Ile1132, Lys1136, Gly1137, Ser1138, Ser1139, Ala1156, Ser1159
B +6UE3	-6.64	Gln1041, Thr1042, Phe1043, His1057, Gly1058, Ile1132, Lys1136, Gly1137, Ser1138, Ser1139, Ala1156, Ser1159
C +6UE3	-6.32	Gln1041, Thr1042, Phe1043, His1057, Gly1058, Leu1135, Lys1136, Gly1137, Ser1138, Ser1139, Arg1155, Ala1156, Ala1157
A +8DK6	-7.16	Gln39, Arg40, Pro41, Glu42, Gln43, Gln44, Ala92, Thr91, Val93, Ser113,Thr115, Glu153
B +8DK6	-7.03	Gln39, Arg40, Pro41, Glu42, Gln43, Gln44, Ala92, Thr91, Val93, Ser113,Thr115, Glu153, Pro154
C +8DK6	-6.03	Gln39, Gln43, Gln44, Lys45, Pro46, Gly47, Gln48, Ala90, Asp91, Tyr95, Lys109, Asp171

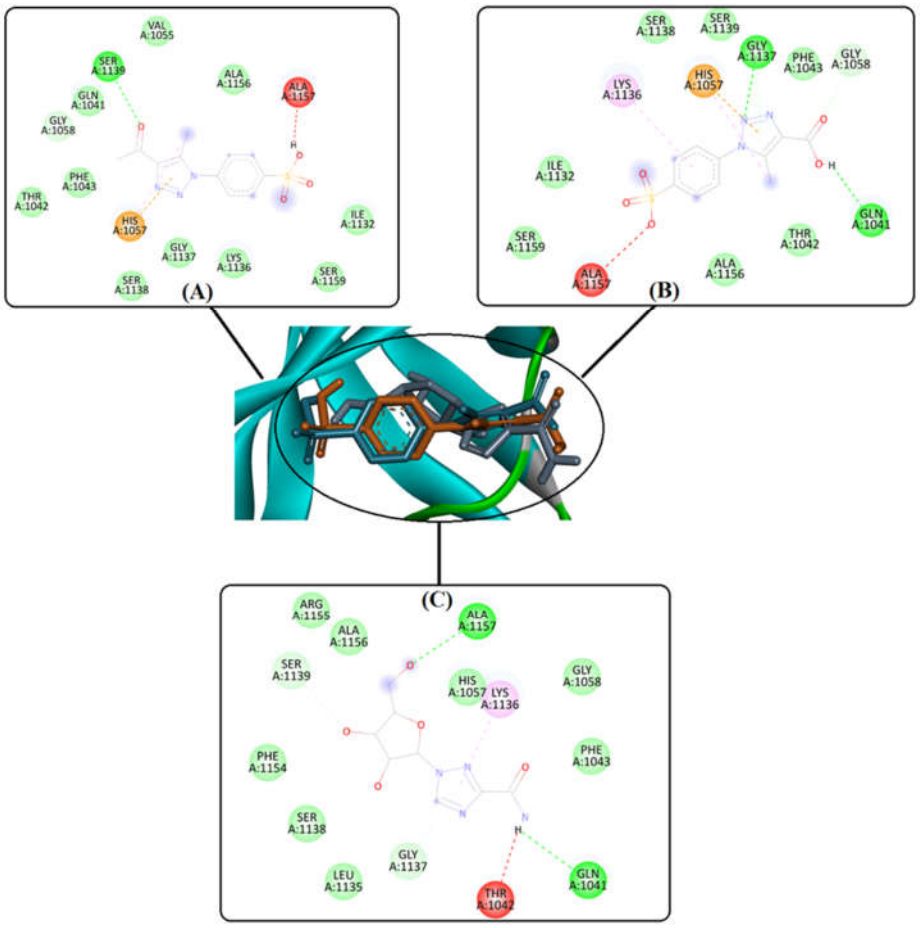

Figure 8. 3D-docking map of (A) structure A, (B) structure B and (C) ribavirin, with the target protein (6UE3) of hepatitis C virus.

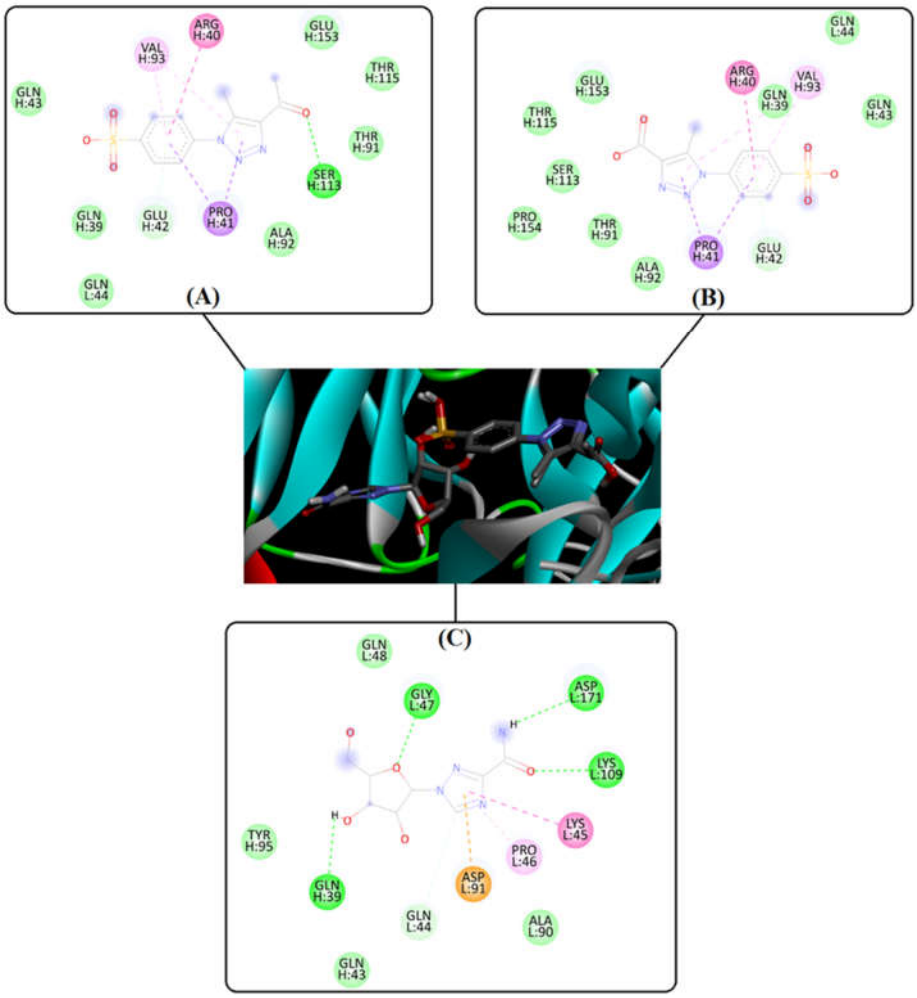

Figure 9. 3D-docking map of (A) structure A, (B) structure B and (C) ribavirin, with the target hepatitis C virus 8DK6.

CONCLUSION

In this study, theoretical calculations were conducted utilizing DFT to examine the derivatives of 1,2,3-triazole ring system. It was noticed that compound A acts as a stronger nucleophile compared to the other ligands due to its ketone group. Theoretically, the investigated compound B demonstrated reactivity in the chemical processes by use of a low energy band gap (2.123 eV), which indicates that further derivatives of this compound could be synthetically feasible. TD-DFT and NCI-RDG analysis predicted the stability of the aromatic system, On the other hand, by conducting molecular docking on the optimized molecules targeting viral proteins (6UE3 and

8DK6), the binding energy indicated the potential inhibition of 8DK6 by both studied compounds in comparison with the control drug (ribavirin).

Data availability

All data and information are available in the manuscript and its supplementary material file.

Ethical approval

Not applicable.

Informed consent

Not applicable.

Conflict of interests and funding

The authors declare that they have no known competing financial interests or personal relationships that could have appeared to influence the work reported in this paper.

REFERENCES

1. Guo, H.Y.; Chen, Z.A; Shen, Q.K; Quan, Z.S. Application of triazoles in the structural modification of natural products. *J. Enzyme Inhib. Med. Chem.* **2021**, 36, 1115-1144.
2. Musa, A.; Abulkhair, H.S.; Aljuhani, A.; Rezki, N.; Abdelgawad, M.A.; Shalaby, K.; El-Ghorab, A.H.; Aouad, M.R. Phenylpyrazolone-1,2,3-triazole hybrids as potent antiviral agents with promising SARS-CoV-2 main protease inhibition potential. *Pharm.* **2023**, 16, 463.
3. Rahman, S.M.A.; Bhatti, J.S.; Thareja, S.; Monga, V. Current development of 1,2,3-triazole derived potential antimalarial scaffolds: Structure- activity relationship (SAR) and bioactive compounds. *Eur. J. Med. Chem.* **2023**, 259, 115699.
4. Mazyed, H.A; Razzaq, A.S; Nahi, R.J. Synthesis and anti-diabetic activity evaluation of new 1,2,3-triazole derivatives incorporating 2-pyrazoline ring. *Int. J. Health Sci.* **2022**, 6, 7299-7309.
5. Rahman, S.M.A.; Bhatti, J.S.; Thareja, S.; Monga, V. Current development of 1,2,3-triazole derived potential antimalarial scaffolds: Structure- activity relationship (SAR) and bioactive compounds. *Eur. J. Med. Chem.* **2023**, 259, 115699.
6. Shaikh, M.H.; Subhedar, D.D.; Khan, F.A.K.; Sangshetti, J.N.; Shingate, B.B. 1,2,3-Triazole incorporated coumarin derivatives as potential antifungal and antioxidant agents. *Chin. Chem. Lett.* **2016**, 27, 295-301.
7. Razzaq, A.S.; Mazyed, H.A.K.; Nahi, R.J. Design, synthesis and evaluation in vitro antibacterial activity of new 1,2,3-triazole derivatives. AIP Conference Proceedings, **2022**. https://doi.org/10.1063/5.0093814.
8. Alam, M.M. 1,2,3-Triazole hybrids as anticancer agents: A review. *Arch. Pharm.* **2021**, 355 e2100158.
9. De Souza-Fagundes, E.M.; Delp, J.; Prazeres, PedroH. D.M.; Marques, L.B.; Carmo, A.M.L.; Stroppa, P.H.F.; Glanzmann, N.; Kisitu, J.; Szamosvàri, D.; Böttcher, T.; Leist, M.; Da Silva, A.D. Correlation of structural features of novel 1,2,3-triazoles with their neurotoxic and tumoricidal properties. *Chem.-Biol. Interact.* **2018**, 291, 253-263.

10. Nemallapudi, B.R.; Guda, D.R.; Ummadi, N.; Avula, B.; Zyryanov, G.V.; Reddy, C.S.; Gundala, S. New methods for synthesis of 1,2,3-triazoles: A review. *PAC* **2021**, 42, 3874-3892.
11. Nahi, R.J. Combination of 1,2,3-triazole, furan and thiazolidin-4-one structures for potential pharmaceutical applications. *Int. J. Pharm. Res.* **2020**, 12, 774-779.
12. Nahi, R.J.; Imran, N.H. Synthesis, characterization and thermal stability study of new heterocyclic compounds containing 1,2,3-triazole and 1,3,4-thiadiazole rings. *Orient. J. Chem.* **2019**, 35, 234-240.
13. Lengerli, D.; Ibis, K.; Nural, Y.; Banoglu, E. The 1,2,3-triazole 'all-in-one'ring system in drug discovery: A good bioisostere, a good pharmacophore, a good linker, and a versatile synthetic tool. *Expert Opin. Drug Discov.* **2022**, 17, 1209-1236.
14. Taher, S.R.; Hamad, W.M. Synthesis, characterization, density functional theory (DFT) analysis, and mesomorphic study of new thiazole derivatives. *Bull. Chem. Soc. Ethiop.* **2024**, 38, 1827-1842.
15. Bootsma, A.N.; Doney, A.C; Wheeler, S.E. Predicting the strength of stacking interactions between heterocycles and aromatic amino acid side chains. *J. Am. Chem. Soc.* **2019**, 141, 11027-11035.
16. Ma, C.M.; Zhao, X.H. Depicting the non-covalent interaction of whey proteins with galangin or genistein using the multi-spectroscopic techniques and molecular docking, *Foods* **2019**, 8, 360.
17. Anighoro, A. Underappreciated chemical interactions in protein–ligand complexes. *Methods Mol. Biol.* **2020**, 2114, 75-86.
18. Yang, J.; Wang, F.; Wang, M.; Wang, D.; Zhou, Z.; Hao, G.; Li, Q.; Yang, G. CIPDB: A biological structure databank for studying cation–π interactions. *Drug Discov. Today* **2023**, 28, 103546.
19. Jemai, N.I.M.; Khalfi, M.; Roisnel, A.S.K.; Al-dossary, H.M.O.; Malyar, Y. Role of non-covalent interactions in novel supramolecular compound, bis(4-phenylpiperazin-1-ium) oxalate dihydrate: synthesis, molecular structure, thermal characterization, spectroscopic properties and quantum chemical study. *Crystals* **2023**, 13, 18.
20. Mohammed, B.A.; Ahmed, S.A.; Al-Healy, F. Design, characterizations, DFT, molecular docking and antibacterial studies of some complexes derived from 4-aminpantipyrine with glycine amino acid ligand. *Bull. Chem. Soc. Ethiop.* **2024**, 38, 1609-1624.
21. Stanzione, F.; Cole, J.C. Use of molecular docking computational tools in drug discovery. *Prog. Med. Chem.* **2021**, 60, 273-343.
22. Nahi, R.J. Combination and molecular docking studies of 1,2,3-triazole and pyrimidin-2-thione rings for potential anti-COVID-19 activity 2023. DOI: 10.19204/2023/XPRN7.
23. Nahi, R.J. Synthesis and molecular docking studies of new pyrimidinone ring containing 1,2,3-triazole derivatives. *Int. J. Drug Deliv. Technol.* **2023**, 13, 1005-1010.
24. Ibraheem, H.H.; Issa A.A.; El-Sayed, D.S. Structural behavior and surface layer modification of (E)-N'-((1H-indol-3-yl) methylene)-4-chlorobenzohydrazide: Spectroscopic, DFT, biomedical activity and molecular dynamic simulation against *Candida albicans* receptor. *J. Mol. Struct.* **2024**, 1312, 138484.
25. Mahmood, W.K.; Dakhal, G.Y.; Younus, D. Comparative properties of ZnO modified Au/Fe nanocomposite: Electronic, dynamic, and locator annealing investigation. *J. Mol. Model.* **2024**, 30, 165.
26. Ibraheem, H.; Al-Majedy, Y.; Issa, A.A.; Yousif, E. Photostabilization, thermodynamic and theoretical studies of polystyrene by some 2-amino pyridine. *Trends Sci.* **2023**, 21, 7374.
27. Issa, A.A.; Alkhafaji, A.A.; Abdulwahid, F.S. Nanocluster-based computational creation of a potential carrier for chemotherapeutic antibacterial drugs. *J. Inorg. Organomet. Polym. Mater.* **2024**, 4713-4728.

28. Mazyed, H.A.; Nahi, R.J. Synthesis and antioxidant study of new1,3-oxazepin-4,7-dione and1,2,3-triazole derivatives. *Int. J. Pharm. Res.* **2020**, 12, 252-259.
29. Parr, R.G. Density-functional theory. *Annu. Rev. Phys. Chem.* **1983**, 34, 631-656.
30. Kadhim, Q.; Abdoon, R.; Mohammed, H.; Abbas, A.; Al-Seady, M.; Nagy, G.; Abduljalil, H.; Saleh, N.A.; Kahaly, M. Effect of metal ad-atoms on the structural, electrical, and optical properties of boron-nitride nanostructures towards optoelectronics: A DFT based study. *Egypt. J. Chem.* **2022**, 65, 745-752.
31. Raghavachari, K. Density-functional thermochemistry. III. The role of exact exchange. *Chem. Phys.* **1993**, 98, 5648-5652.
32. Dennington, R.; Keith, T.A.; Millam, J.M. GaussView, version 6.0. 16. Semichem Inc Shawnee Mission KS, **2016**, 13(1).
33. Hanwell, D.C.M.D.; Curtis, D.E.; Lonie, E.; andermeersch, T.V.; Hutchison, G.R. Avogadro: An advanced semantic chemical editor, visualization, and analysis platform. *J. Cheminform.* **2012**, 4, 1-17.
34. El-Sayed, D.S.; Tawfik, E.M.; Elhusseiny, A.F.; El-Dissouky, A.A. Perception into binary and ternary copper(II) complexes: synthesis, characterization, DFT modeling, antimicrobial activity, protein binding screen, and amino acid interaction. *BMC Chem.* **2023**, 17, 1-21.
35. Matthew, A.N.; Zephyr, J.; Rao, D.N.; Henes, M.; Kamran, W.; Kosovrasti, K.; Schiffera, C.A. Avoiding drug resistance by substrate envelope-guided design: Toward potent and robust HCV NS3/4A protease inhibitors. *Mol. Biol. Physiol.* **2020**, 11, 1-15.
36. Kumar, A.; Tiana, R.; Elizabeth, J.K. Regions of hepatitis C virus E2 required for membrane association. *Nat. Commun.* **2023**, 14, 1-10.
37. Trott, O.; Olson, A.J; AutoDock Vina: Improving the speed and accuracy of docking with a new scoring function, efficient optimization, and multithreading. *J. Comput. Chem.* **2010**, 31, 455-461.
38. Mohammed, H.T.; Kamil, A.H.; Abduljalil, H.M.; Drea, A.A.; Al-Seady, M.A. Degradation of indigo dye using quantum mechanical calculations. *Baghdad Sci. J.* **2023**, 20, 1352.
39. Ryu, S.R.; Noda, I.; Jung, Y.M. Relationship between infrared peak maximum position and molecular interactions. *Bull. Korean Chem. Soc.* **2011**, 32, 4011-4015.
40. Al-Seady, M.A.; Abed, H.H.; Alghazaly, S.M. Prospective utilization of boron nitride and beryllium oxide nanotubes for Na, Li, and K-ion batteries: A DFT-based analysis. *J. Mol. Model.* **2023**, 29, 348.
41. Abdulsattar, M.A.; Abduljalil, H.M.; Abed, H.H. Temperature and humidity effects on the acetone gas sensing of pristine and Pd-doped WO_3 clusters: A transition state theory study. *J Mol. Model.* **2024**, 30, 215.
42. Alsaati, S.; Abdoon, R.S.; Hussein, E.H. Unveiling the potential of graphene and S-doped graphene nanostructures for toxic gas sensing and solar sensitizer cell devices: Insights from DFT calculations. *J. Mol. Model.* **2024**, 30, 191.
43. Venkataramanan, N.S.; Suvitha, A.; Kawazoe, Y. Unravelling the nature of binding of cubane and substituted cubanes within cucurbiturils: A DFT and NCI study. *J. Mol. Liq.* **2018**, 260, 18-29.
44. Chou, J.C.; Buehler, M.J. Bond energy effects on strength, cooperativity and robustness of molecular structures. *Interface Focus* **2011**, 1, 734-743.
45. Rajan, S.; Baek, K.; Yoon, H. C-H… O hydrogen bonds in FK506-binding protein–ligand interactions. *J. Mol. Recognit.* **2013**, 26, 550-555.